

Research on Engineering Structures & Materials



www.jresm.org



Flow of non-Newtonian fluids in self-similar networks across different scales

Antonio F. Miguel

Online Publication Date: 10 January 2025

URL: http://www.jresm.org/archive/resm2025-474ma1005rs.html

DOI: http://dx.doi.org/10.17515/resm2025-474ma1005rs

Journal Abbreviation: Res. Eng. Struct. Mater.

To cite this article

Miguel A F. Flow of non-Newtonian fluids in self-similar networks across different scales. *Res. Eng. Struct. Mater.*, 2025; 11(5): 2253-2266.

Disclaimer

All the opinions and statements expressed in the papers are on the responsibility of author(s) and are not to be regarded as those of the journal of Research on Engineering Structures and Materials (RESM) organization or related parties. The publishers make no warranty, explicit or implied, or make any representation with respect to the contents of any article will be complete or accurate or up to date. The accuracy of any instructions, equations, or other information should be independently verified. The publisher and related parties shall not be liable for any loss, actions, claims, proceedings, demand or costs or damages whatsoever or howsoever caused arising directly or indirectly in connection with use of the information given in the journal or related means.



Published articles are freely available to users under the terms of Creative Commons Attribution - NonCommercial 4.0 International Public License, as currently displayed at here (the "CC BY - NC").



Research on Engineering Structures & Materials



www.jresm.org

Research Article

Flow of non-Newtonian fluids in self-similar networks across different scales

Antonio F. Miguel *,1,2,a

¹Complex Flow Systems Lab, University of Evora, Portugal ²Institute of Earth Sciences, the branch of Evora, Portugal

Article Info

Abstract

Article history:

Received 05 Oct 2024 Accepted 01 Jan 2025

Keywords:

Flow systems; Scale-invariance; Self-similarity; Prefractal dimension; Flow resistance; Non-newtonian fluids Several natural and manufactured flow systems exhibit scale-invariance or selfsimilarity, despite appearing to be disordered. This study focuses on the laminar flow of non-Newtonian fluids through self-similar systems of tubes with porous walls (intrinsic permeability much less than 10-4 m²). Two arrangements of tubes are discussed: a dendritic flow structure and a bundle of tubes. The size of these arrangements is described as a function of structural parameters for both straight and tortuous tubes, and the flow resistance is obtained as a function of structural parameters and fluid properties. Among other findings, it is shown that the prefractal dimension of dendritic networks for maximum flow access is dependent on the size constraint chosen to design the network. Results also show that as the prefractal dimensions of diameters and lengths rise, so does the overall size of the dendritic network and tube bundle system. In contrast, it is observed that the flow resistance diminishes as the prefractal dimension for diameters increases, whereas for tortuous tubes the flow resistance increases as the prefractal dimension for lengths increases. The approaches presented in this paper have numerous potential applications, including fluxes in biological systems, microfluidic media, and hydrology.

© 2025 MIM Research Group. All rights reserved.

1. Introduction

Fluid flow through complex networks of pores/tubes is common both in man-made and natural systems [1-3]. Fluid properties and the geometry through which the fluid circulates are crucial to establish the characteristics of the flow [3]. Therefore, diffusion coefficients and viscosities are properties of ample practical interest as well as the internal shape and structure of flow sites and their connectivity between them. In systems with specific geometries, the Euclidean dimension is insufficient to properly represent the system, hence the concept of prefractal was established [4-7]. Thus, for systems that have statistical self-similarity across a variety of scales, a measure of the complexity of the lengths/times that characterize these systems is obtained based on the so-called prefractal dimension. Prefractals are characterized by power laws with non-integer or integer exponents [4,5]. These scale-invariant systems are ubiquitous in nature and feature diverse man-made systems.

From a fundamental perspective, fluid flow in permeable media raises interesting challenges, particularly concerning the prefractal geometry of open space. Several attempts have been made to explain how the prefractal features of media affect fluid flow [7-10]. These attempts can be divided into two categories: one related to the flow represented by conventional flow equations through a prefractal open space, and the other

^{*}Corresponding author: $\underline{\mathsf{afm}@uevora.pt}$

^a orcid.org/0000-0001-6287-2056

to the flow network related to a continuum flow driven by nonconventional (prefractal) flow equations. A comprehensive review of the recent development of prefractal design of flow systems is provided by Babadagli [11].

This paper is based on the methodology presented in the articles of Miguel et al. [12,13] and presents analytical models for two different configurations: one composed of a self-similar dendritic network of porous tubes, and the other composed of a self-similar arrangement of porous tubes embedded in a porous material (intrinsic permeability less than $10^{-4} \, \text{m}^2$), whose dimensions follow scaling laws. Our study considers non-Newtonian fluid flows and relies on the power law approach (Ostwald de Waele fluid) to estimate the variations in the fluid viscosity due to the applied shear rate. Power-law fluids are used in a variety of applications, including biological flow systems, microfluidic media, and engineering systems.

2. Theory

2.1. Fluid Flow Through a Tube with Porous Wall

Consider a time-independent laminar flow, axisymmetric through a cylindrical tube with rigid and impervious wall. According to Navier-Stokes equations, the flow of a Newtonian fluid is given by;

$$\frac{\mathrm{dp/dz}}{\mu Q} = \frac{8s_{\mathrm{f}}}{D^4} \tag{1}$$

which is known as the Hagen–Poiseuille equation. Here Q is the volumetric flow rate, s_f is a shape factor $(16/\pi)$, D is the diameter, z is a space variable, p is the pressure, and μ is the dynamic viscosity.

Now consider that the tube's wall is made of pores and has constant intrinsic permeability. Assuming that the exterior pressure is considered constant (i.e., a reference pressure $p_{ext} = 0$), the permeation flow is not constant due to the tube's inner pressure. Differentiating Eq. (1) yields;

$$\frac{dQ}{dz} = -\frac{D^4}{8\mu s_r} \frac{d^2p}{dz^2} \tag{2}$$

As the Darcy law governs the creeping fluid flow through the wall, the fluid flow variation along the tube is given by;

$$\frac{dQ}{dz} = \frac{dQ_p}{dz} = -\pi D \frac{k}{\mu} \frac{p}{l}$$
 (3)

where k is the intrinsic permeability and l is the wall thickness. Substitution of Eq. (3) into Eq. (2) yields;

$$\frac{d^2p}{dz^2} - \frac{8\pi s_f k}{D^3 l} p = 0 \tag{4}$$

which has a solution of the form $p(z) = a_1 \exp(-bz) + a_2 \exp(bz)$, where a_1 , a_2 and b are constants [14]. Middleman [15] and Vassilieff [16] noticed that the pressure with respect to the axial position experiences a slight curve. Since the properties of the fluid and the geometric characteristics of the tube are constant, both the above solution or a parabolic pressure solution of type $p(z)=c_1+c_2$ $z+c_3z^2$ can be applied [15]. Accounting for the

continuity equation, and that $dp/dz=8s_f\mu Q_{in}/D^4$ and at inlet the pressure is p_{in} , the pressure variation along the length of the tube can be written as;

$$p(z) - p_{in} = \frac{8s_f \mu Q_{in}}{\rho D^4} z \left[1 + \frac{3k}{2Q_{in}} \left(\frac{p_{in} \rho D^4 - 64\mu L Q_{in}}{3D^3 - 64\mu k L^2} \right) z \right]$$
 (5)

The pressure difference between the outlet and the inlet of the tube is;

$$p_{L} - p_{in} = \frac{8s_{f}\mu LQ_{in}}{\rho D^{4}} \left[1 + \frac{3Lk}{2Q_{in}} \left(\frac{p_{in}\rho D^{4} - 64\mu LQ_{in}}{3D^{3} - 64\mu kL^{2}} \right) \right]$$
 (6)

Note that the Hagen-Poiseuille equation is obtained when the intrinsic permeability of the tube walls is zero.

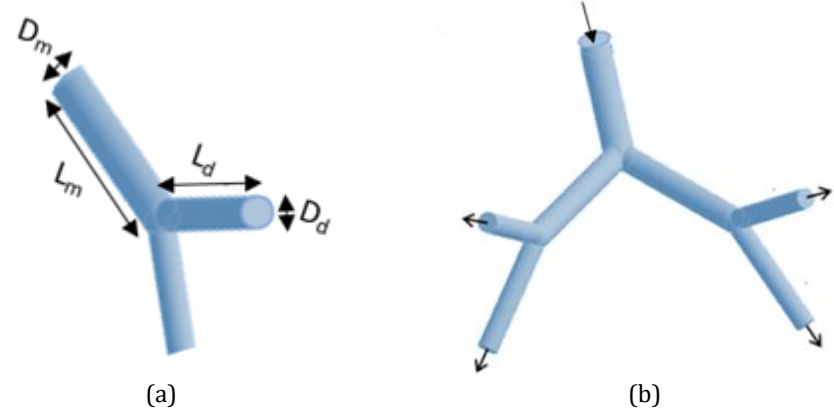


Fig. 1. The base system consists of a tube that splits into two tubes (a) to form a network of dendritic tubes (b)

2.2. Flow through Bifurcated Tubes of a Newtonian Fluid

Consider a symmetric configuration composed of a tube that bifurcates into two daughter tubes (Fig. 1a). Defining the flow resistance as the ratio between fluid flow and pressure difference, the total flow resistance of the configuration of tubes is [6];

$$R = R_m + \frac{1}{2} R_d \tag{7}$$

with:

$$R_{m} = \frac{s_{f} \mu L_{m}}{D_{m}^{4}} \left[1 + \frac{3L_{m}k}{2Q_{in}} \left(\frac{p_{in} \rho D_{m}^{4} - 64\mu L_{m} Q_{in}}{3D_{m}^{3} - 64\mu k L_{m}^{2}} \right) \right]$$
(8)

$$R_{d} = \frac{s_{f} \mu L_{d}}{D_{d}^{4}} \left\{ 1 + \frac{3L_{d}k}{(Q_{in} - Q_{k})} \left[\frac{p_{in,d} \rho D_{d}^{4} - 32\mu L_{d}(Q_{in} - Q_{k})}{3D_{d}^{3} - 64\mu k L_{d}^{2}} \right] \right\}$$

$$(9)$$

where the subscripts m and d mean parent and daughter tubes, respectively. The total size of this bifurcated system is given by;

$$S = s_s D_m^w L_m + 2s_s D_d^w L_d \tag{10}$$

where w takes a value of 1 or 2 for the lateral area and volume, respectively, and s_s is a shape factor equal to π for the lateral area and to $\pi/4$ for the volume. Consider that this bifurcated flow system is repeated over multiple spatial scales (Fig. 1b). Since self-similarity is a characterizing property, two crucial characteristics of the flow network are observed: the bifurcation of tubes and the decrease in the diameter of tubes (and cross-sectional area) from one level to the next in the tree. This can be approached by;

$$D_i = \alpha^j D_0$$
 $j = 1, 2, ...n$ (11)

where the scaling factor for diameters or magnification factor α (a constant for the dendritic network) can be related to the number of bifurcating tubes n and the prefractal dimension d_f according to;

$$\alpha = c_o n^{-\frac{1}{d_f}} \tag{12}$$

where c_0 is a constant. This power-law relationship ensures that the design of the tubes appears the same across different length scales of observation. A measure of the change of n can be obtained by differentiating Eq. (11) with respect to D_i ;

$$\frac{dn}{n} = -d_f \frac{dD_j}{jD_j} \tag{13}$$

This result shows that n and D_j vary in opposite ways, that is, when one of them increases the other decreases. As a result, a self-similar dendritic network of tubes is composed of a few large-diameter tubes and many small-diameter tubes.

The diameter of the tubes that comprise each bifurcation level is related to the flow resistance. For a minimum flow resistance under space constraint, the following relationship must be verified [6];

$$\frac{\partial R}{\partial D_m} \frac{\partial D_m}{\partial D_d} + \frac{\partial R}{\partial D_d} = 0 \tag{14}$$

with the $\partial D_m/\partial D_d$ obtained from the space constraint given by Eq. (10). According to Eqs. (7), (10), and (14), the relationship between daughter and parent diameters for minimum flow resistance is given by;

$$\frac{D_d}{D_m} = \left\{ \frac{\left[28672(\mu k L_m^2)^2 - 3552\mu k L_m^2 D_m^3 + 36D_m^6 + \frac{27\rho}{2Q_m} p_{in} L_m k D_m^7 \right]^{\frac{1}{2}} \left(64\mu k L_d^2 - 3D_d^3 \right)}{\left[40960(\mu k L_d^2)^2 - 3552\mu k L_d^2 D_d^3 + 36D_d^6 + 27\rho (Q_{in} - Q_k)^{-1} p_{in,d} L_d k D_d^7 \right]^{\frac{1}{2}} \left(64\mu k L_m^2 - 3D_m^3 \right)} \right\}^{\frac{2}{4+w}}$$
(15)

Eq. (14) is implicit and needs to be solved iteratively. For $k<10^{-4}$ m², the previous equation's k-dependent terms are significantly less than the other terms and can be ignored (refer to the results of section 3.1). Then, the previous equation can be expressed as;

$$\frac{D_d}{D_{--}} = 2^{-\frac{2}{4+w}} \tag{16}$$

Using a similar process and replacing D by L in Eq. (14), the optimal length ratio (i.e., length ratio for minimum flow resistance) is given by;

$$\frac{L_d}{L_m} = 2^{\frac{1+w}{4+w}} \tag{17}$$

2.3. Flow through Bifurcated Tubes of a non-Newtonian Fluid

Because of its effectiveness and simplicity, we use the Hagen-Poiseuille equation (laminar flow) and a power law to account for variations in fluid viscosity caused by the applied shear rate. The Ostwald de Waele power law is a well-known model because a wide variety of problems were solved based on this approach. For $k << 10^{-4} \text{ m}^2$, the flow resistance of a single tube can be obtained as;

$$R = \frac{2^{3\chi+4} \left(\frac{3\chi+1}{4\chi}\right)^{\chi} KL}{\pi^{\chi} D^{3\chi+1}} Q^{\chi-1}$$
(18)

where Q is the volumetric flow rate, K is the consistency of fluid, and χ is the fluid behavior index (χ <1 the fluid is named pseudoplastic or shear thinning, χ >1 the fluid is called dilatant or shear thickening, and for χ =1 the Newtonian fluid is obtained).

The resistance of a system composed of a parent tube that branches into 2 symmetric daughter tubes is;

$$R = \left(\frac{3\chi + 1}{4\chi}\right)^{\chi} \frac{KQ^{\chi - 1}}{\pi^{\chi}} \left[\frac{2^{3\chi + 4}L_m}{D_m^{3\chi + 1}} + \frac{2^{2\chi + 4}L_d}{D_d^{3\chi + 1}} \right]$$
(19)

Using a methodology akin to that described in the preceding section, the optimal size ratios for a tube that splits into two tubes (Fig. 1a) are;

$$\frac{D_d}{D_m} = 2^{\frac{-(\chi+1)}{3\chi+w+1}} \tag{20}$$

$$\frac{L_d}{L_m} = 2^{\frac{3\chi^2 - 3\chi - 2}{3\chi + w + 1}} \tag{21}$$

Note that when χ =1 the allometric relations for Newtonian fluids (Eqs. 16 and 17) are obtained.

2.3.1 Geometric Characteristics for Minimum Flow Resistance and Prefractal Dimension

The ratio of diameters and lengths for the least resistance of fluid flow under surface area and volume constraints is illustrated by the allometric Eqs. (20) and (21). Eqs. (11), (12), (20) and (21) provide the following definition of the prefractal dimension;

$$d_{D} = \frac{3\chi + w + 1}{\chi + 1} \tag{22}$$

$$d_{fL} = \frac{3\chi + w + 1}{2 + 3\chi - 3\chi^2} \tag{23}$$

According to these equations, both the prefractal dimension for diameters ($d_{\mathbb{D}}$) and lengths ($d_{\mathbb{L}}$) depend on the constraints of the system and the fluid behavior index. For example, $d_{\mathbb{D}}$ for a Newtonian fluid is 2.5 or 3.0, depending on whether the constraint is the tube's lateral area or volume, respectively.

The total size and the total resistance of the bifurcated system of tubes (Eqs. 10 and 19, Fig. 1a) can be written in terms of prefractal dimensions as;

$$S = s_s D_m^w L_m \left(1 + 2^{1 - \frac{w}{d_{fD}} - \frac{1}{d_{fL}}} \right)$$
 (24)

$$R = \frac{KQ^{\chi - 1}}{\pi^{\chi}} \frac{L_{m}}{D_{m}^{3\chi + 1}} \left(\frac{3\chi + 1}{4\chi} \right)^{\chi} \left(1 + 2^{3\chi + 4 + \frac{3\chi + 1}{d_{JD}} - \frac{1}{d_{JL}}} \right)$$
 (25)

For example, for a network composed of j-levels of bifurcated tubes (Fig. 1b), the total size of tubes is given by;

$$S = \sum_{i=0}^{j} s_{s} 2^{i} D_{i}^{w} L_{i} = s_{s} D_{0}^{w} L_{0} \frac{1 - \left[2 \frac{L_{1}}{L_{0}} \left(\frac{D_{1}}{D_{0}} \right)^{w} \right]^{j+1}}{1 - \left[2 \frac{L_{1}}{L_{0}} \left(\frac{D_{1}}{D_{0}} \right)^{w} \right]} = s_{s} D_{0}^{w} L_{0} \frac{1 - \left[2^{\frac{1 - w}{d_{jD}} - \frac{1}{d_{fL}}} \right]^{j+1}}{1 - 2^{\frac{1 - w}{d_{jD}} - \frac{1}{d_{fL}}}}$$

$$(26)$$

where d_{fD} and d_{fL} are given by Eqs. (22) and (23), respectively.

2.4. Fluid Flow Through Self-Similar Arrangement of Tubes

Consider a system composed of tubes with varied cross-sectional diameters (Fig. 2). Let L be the length of the material which has a self-similar distribution of tubes with diameters ranging from minimum diameters D_{min} and maximum diameters D_{max} (i.e., $D_{min} \le D \le D_{max}$ and $D_{min} <<< D_{max}$). Using an approach similar to those shown in the previous section (Eq. 11 and 12), we can write [4,12,13];

$$D = \beta D_{\text{max}} \tag{27}$$

with the scaling factor for diameters given by;

$$\beta = N(\geq D)^{-\frac{1}{d_{p_0}}} \tag{28}$$

where N is the number of tubes having a diameter equal to or greater than D. Differentiating this equation yields;

$$\frac{dN(\geq D)}{N(\geq D)} = -d_{fD}\frac{dD}{D_{max}} \tag{29}$$

This equation, like Eq. (13), shows that the number of tubes in the flow system reduces as the diameter increases. As a consequence, a self-similar arrangement of tubes consists of many small-diameter tubes and a small number of larger-diameter tubes [4].

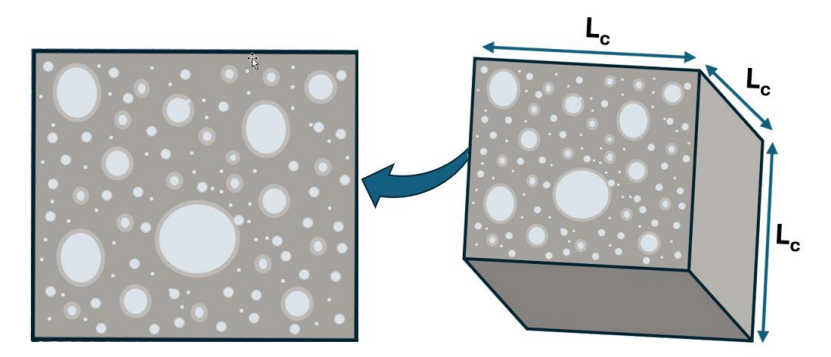


Fig. 2. Self-similar arrangement of tubes that are independent of one another

2.4.1 Size and Fluid Flow Resistance of An Arrangement of Straight Tubes

Consider that the arrangement of tubes in the Fig. 2 is composed of straight-length tubes. Taking into account Eqs. (27) to (29), the total volume of the tubes is given by;

$$S = \int_{D_{\min}}^{D_{\max}} s_s D^2 L_c(dN(\geq D)) = \int_{D_{\min}}^{D_{\max}} s_s L_c d_{fD} D_{\max}^{d_{fD} - 1} D^{2 - d_{fD}} dD$$
(30)

Integrating the previous equation yields;

$$S = \frac{s_s L_c d_{fD} D_{\text{max}}^2}{3 - d_{fD}} \left[1 - \left(\frac{D_{\text{min}}}{D_{\text{max}}} \right)^{3 - d_{fD}} \right]$$
 (31)

Using a similar process, for $k << 10^{-4} \text{ m}^2$ the total flow resistance of the arrangement of tubes is given by;

$$Q = \int_{D_{\min}}^{D_{\max}} -\frac{c_{\chi} \Delta p^{\frac{1}{\chi}} d_{fD} D_{\max}^{d_{fD} - 1} D^{\frac{\chi(3 - d_{fD}) + 1}{\chi}}}{\frac{1}{L_c^{\chi}}} dD$$
(32)

and the flow resistance is;

$$R = \frac{Q^{\chi - 1} L_{c}}{\left\{ \frac{\chi c_{\chi} d_{D}}{\chi \left(4 - d_{D} \right) + 1} D_{\max}^{3 + \frac{1}{\chi}} \left[1 - \left(\frac{D_{\min}}{D_{\max}} \right)^{4 - d_{D} + \frac{1}{\chi}} \right] \right\}^{\chi}} = \frac{c_{R} L_{c} \operatorname{Re}_{MR}^{\frac{\chi - 1}{2 - \chi}} D_{\max}^{\frac{(4 - 3\chi)(\chi - 1)}{2 - \chi}}}{\left\{ \frac{\chi c_{\chi} d_{D}}{\chi \left(4 - d_{D} \right) + 1} D_{\max}^{3 + \frac{1}{\chi}} \left[1 - \left(\frac{D_{\min}}{D_{\max}} \right)^{4 - d_{D} + \frac{1}{\chi}} \right] \right\}^{\chi}}$$
(33)

with;

$$c_{R} = \frac{\pi^{\chi - 1} \left(\frac{3\chi + 1}{4\chi}\right)^{\frac{\chi(\chi - 1)}{2 - \chi}} K^{\frac{\chi - 1}{2 - \chi}}}{2^{\frac{2(4 - 3\chi)(\chi - 1)}{2 - \chi}} \rho^{\frac{\chi - 1}{2 - \chi}}}$$
(34)

$$Re_{MR} = \frac{2^{2(4-3\chi)}\rho Q^{2-\chi}}{\pi^{2-\chi} D_{\max}^{4-3\chi} \left(\frac{3\chi+1}{4\chi}\right)^{\chi} K}$$
(35)

where Re_{MR} is the Metzner–Reed Reynolds number, and S and R are the total size of the tubes and the total resistance of the tubes, respectively.

2.4.2 Size and Fluid Flow Resistance of An Arrangement of Tortuous Tubes

Tortuous describes the sinuosity of the tube in space, and tortuosity can be defined as the ratio of tube curve length over the line distance between the two ends. Consider that the tubes' length is tortuous rather than straight ($L \ge L_c$). Tube diameters satisfy Eqs. (27) and (28), whereas the following scaling equations describe tube lengths that follow self-similarity [13];

$$L = \theta L_c \tag{36}$$

with the scaling factor given by:

$$\theta = \left(\frac{D}{L_c}\right)^{1-d_{gL}} \tag{37}$$

where d_{fL} is the prefractal dimension of the tortuous tubes. In this case, the total volume of the tortuous tubes is given by;

$$S = \int_{D_{\min}}^{D_{\max}} s_s L_c^{d_{fl}} d_{fD} D_{\max}^{d_{fD}-1} D^{3-d_{fD}-d_{fl}} dD$$
(38)

After integration, the above equation yields;

$$S = \frac{s_s L_c^{d_{gl}} d_{gD} D_{\text{max}}^{3-d_{gl}}}{4 - d_{gD} - d_{gl}} \left[1 - \left(\frac{D_{\text{min}}}{D_{\text{max}}} \right)^{4 - d_{gD} - d_{gl}} \right]$$
(39)

The resistance can be obtained in the same manner as described in the preceding section. Assuming that the intrinsic permeability is much less than 10^{-4} m²;

$$Q = \int_{D_{\min}}^{D_{\max}} -\frac{c_{\chi} \Delta p^{\frac{1}{\chi}} d_{fD} D_{\max}^{d_{fD} - 1} D^{\frac{\chi(3 - d_{fD}) + d_{fL}}{\chi}}}{L^{\frac{d_{fL}}{\chi}}} dD$$
(40)

and the total flow resistance is;

$$R = \frac{Q^{\chi - 1} L_{c}}{\left\{ \frac{\chi c_{\chi} d_{D}}{\chi \left(4 - d_{D} \right) + d_{D}} D_{\max}^{3 + \frac{d_{D}}{\chi}} \left[1 - \left(\frac{D_{\min}}{D_{\max}} \right)^{4 - d_{D} + \frac{d_{D}}{\chi}} \right] \right\}^{\chi}} = \frac{c_{R} L_{c} \operatorname{Re}_{MR}^{\frac{\chi - 1}{2 - \chi}} D_{\max}^{\frac{\chi - 1}{2 - \chi}} \left[1 - \left(\frac{D_{\min}}{D_{\max}} \right)^{4 - d_{D} + \frac{d_{D}}{\chi}} \right]^{\chi}}{\left\{ \chi \left(4 - d_{D} \right) + d_{D} D_{\max}^{3 + \frac{d_{D}}{\chi}} \left[1 - \left(\frac{D_{\min}}{D_{\max}} \right)^{4 - d_{D} + \frac{d_{D}}{\chi}} \right] \right\}^{\chi}}$$

$$(41)$$

It should be noted that for tubes of non-tortuous length, the prefractal dimension d_{fL} is 1, and Eqs. (31) and (33) are obtained again.

3. Results and Discussion

3.1. Fluid Flow in Porous Wall Bifurcated Tubes Designed with Minimum Flow Resistance

Fig. 3 illustrates how the ratio of the daughter tube to the parent-daughter tube diameters (Fig. 1a), for minimum flow resistance, varies with the k, w, and L_d/L_m . Regardless of the intrinsic permeability of the walls and the ratio between the lengths of the daughter tubes and the parent tube, we may conclude that D_d/D_m depends on w which represents the type of space constraint imposed on the system. Additionally, for an intrinsic permeability of less than 10^{-4} m², D_d/D_m remains independent of L_d/L_m . Then, the ratio of diameters that is only dependent on the constraint w is given by $D_d/D_m = 2^{-2/4+w}$ (for k<10-4 m2). Additionally, it should be mentioned that for volume constraint (w=2) the ratio of the diameters D_d/D_m is larger than for lateral area constraint (w=1).

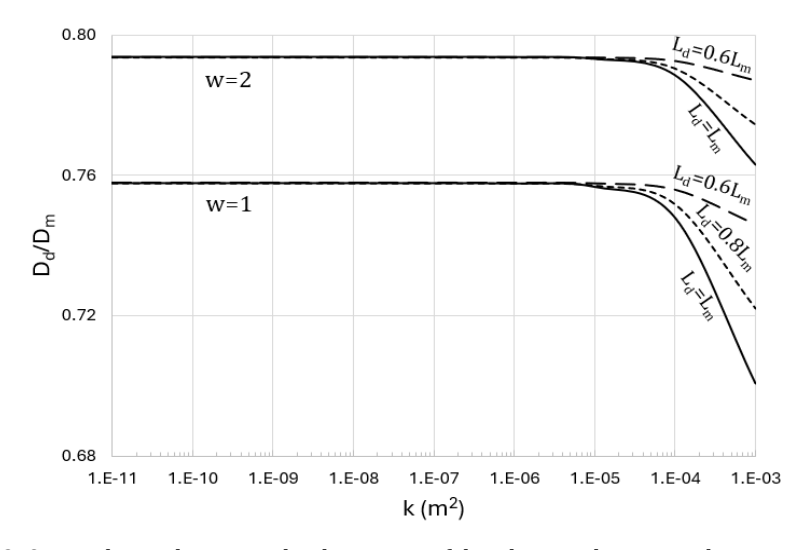


Fig. 3. Optimal ratio between the diameters of daughter and parent tubes versus the intrinsic permeability of porous wall (Eq. 15)

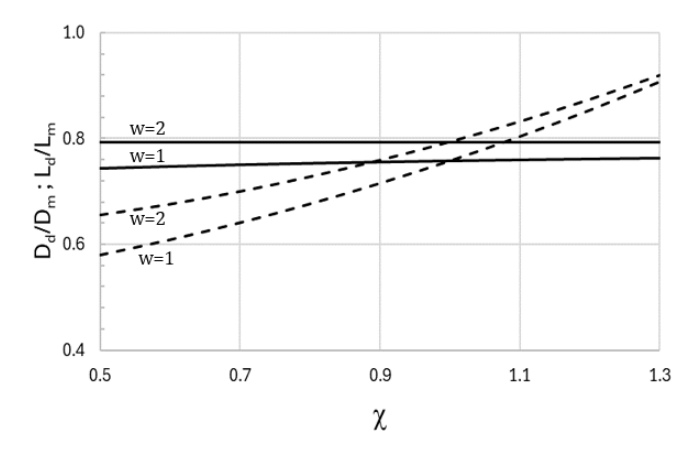


Fig. 4. Ratios between the diameters of daughter and parent tubes D_d/D_m (—, Eq. 20) and between the lengths of daughter and parent tubes L_d/L_m (---, Eq. 21) versus fluid behavior index γ and the geometric constraint w

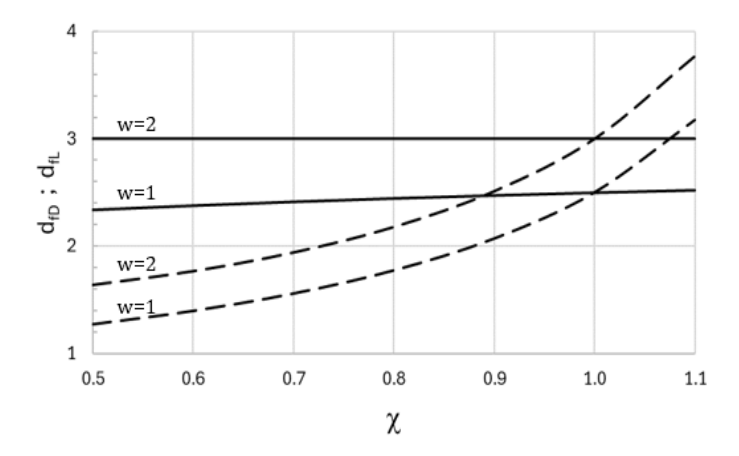


Fig. 5. Prefractal dimension for diameters d_{fD} (—, Eq. 22) and lengths d_{fL} (---, Eq. 23) versus fluid behavior index γ and the geometric constraint w

For branching systems designed with minimum flow resistance, Figs. 4 and 5 depict the variation of the size ratios and the prefractal dimensions with respect to the fluid behavior index χ and the geometric factor w. Fig. 4 indicates that the diameter and length ratios are greater for volume constraint than lateral area constraint. Besides, the length ratio grows with the fluid behavior index, but the diameter ratio remains relatively constant. The same tendency of variation with w and χ recorded for the size ratios occurs for the prefractal dimensions $d_{\rm ID}$ and $d_{\rm fL}$ (Fig. 5).

3.2. Fluid Flow Through a Dendritic Network of Tubes

Consider now the design's base unit for dendritic flow networks, which consists of a parent tube that bifurcates into two daughter tubes. Figs. 6 and 7 show the dimensionless total size (Eq. 24) and the dimensionless total flow resistance (Eq. 25). Fig. 6 indicates that increasing the prefractal dimension for diameters or the prefractal dimension for lengths increases the network's overall size.

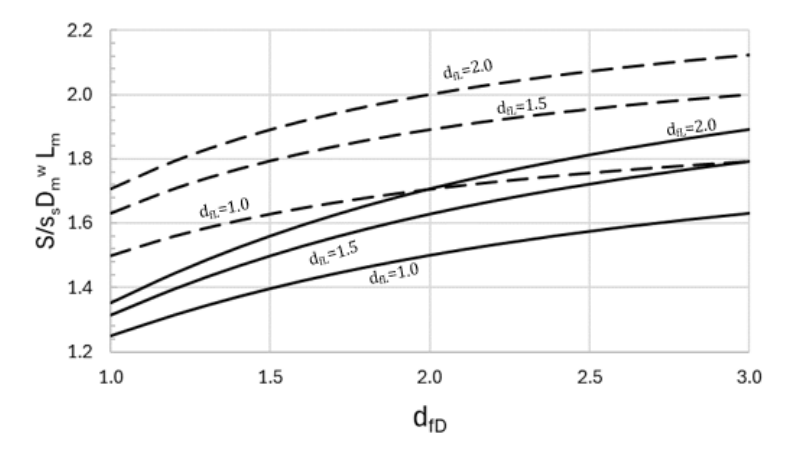


Fig. 6. Dimensionless total size of network versus the prefractal dimensions (d_{fD} and d_{fL}) and the geometric constraints (w=1 (---) and w=2 (–))

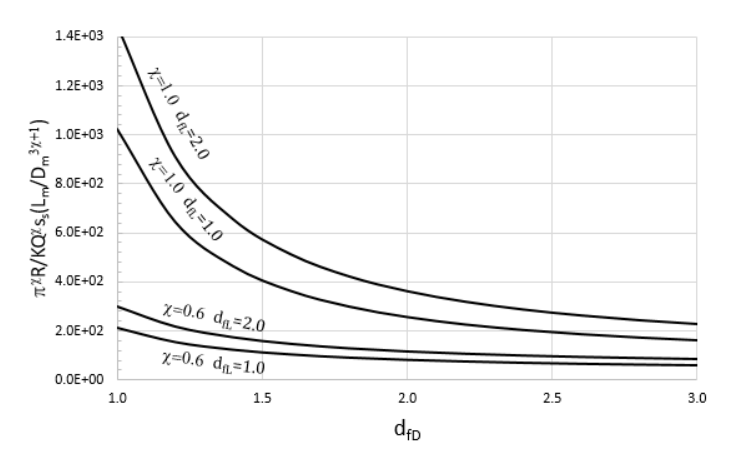


Fig. 7. Dimensionless total flow resistance of network versus the prefractal dimensions $(d_{\mathbb{D}}$ and $d_{\mathbb{R}})$ and the fluid behavior index χ .

The system size is larger when the constraint is the lateral area. However, the dimensionless total flow resistance decreases as the prefractal dimension for diameters increases, and it increases as the prefractal dimension for lengths increases (Fig. 7). An increase in the fluid behavior index also increases dimensionless resistance.

3.3. Fluid Flow Fluid Through Self-Similar Arrangement of Tubes

For the system depicted in Fig. 2, Eqs. (39) and (41) are plotted in Figs. 8 and 9. The dimensionless total size of tubes increases as the prefractal dimensions ($d_{\rm ID}$ and $d_{\rm fL}$) increase. It is also worth noting that only when the tube diameter's fractal dimension exceeds two does the $d_{\rm fL}$ become significant. Regarding the dimensionless flow resistance of the system of tubes, the increase in prefractal dimensions ($df_{\rm D}$ or $df_{\rm L}$) raises the total dimensionless resistance. Furthermore, the dimensionless resistance to flow increases for fluids with a higher fluid behavior index.

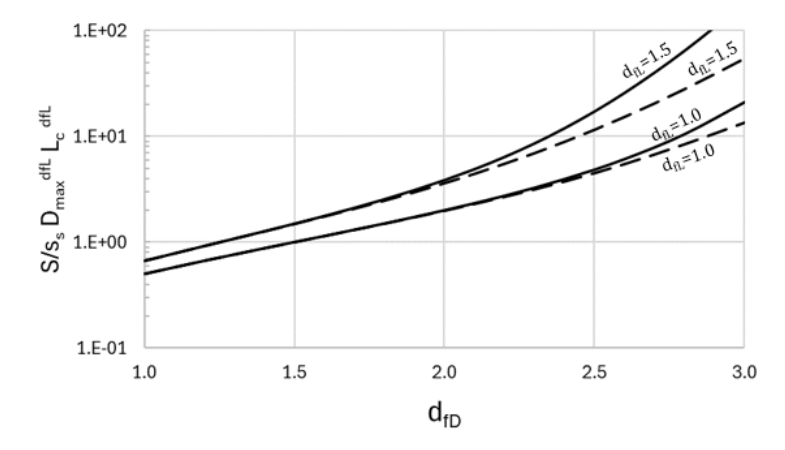


Fig. 8. Dimensionless total size of tubes versus the prefractal dimensions (d_{ID} and $d_{\text{fl.}}$) and the geometric constraints (w=1 (---) and w=2 (-))

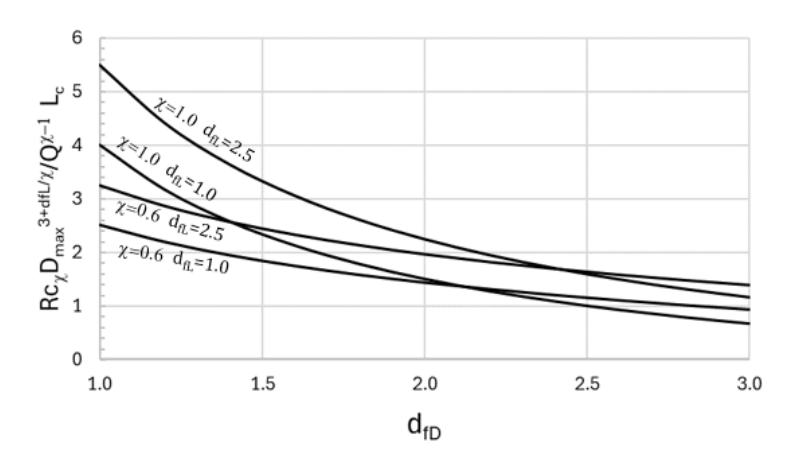


Fig. 9. Dimensionless total flow resistance of tubes versus the prefractal dimensions $(d_{ID}$ and $d_{fL})$ and the fluid behavior index χ .

Variations in the prefractal dimension of biological systems are often linked to changes in the way they operate. The above figures may be useful in understanding why changes in the prefractal dimension of biological systems may be connected with changes in the system's operation.

The prevalence of osteoporosis, for example, is related to an increase in prefractal dimension [17]. Healthy bones have a prefractal dimension of about 2.60, while severe osteoporosis has a prefractal value of around 2.95. This means that a larger prefractal dimension results in a larger size of empty spaces (Figs. 6 and 8). Thus, as the prefractal dimension rises, the open space expands, which may contribute to a decrease in structural strength, but it's not the only issue. The ability to produce blood cells is also compromised (less material, more open gaps), which is also a major concern.

Understanding other conditions can be aided by a similar perception based on Figs. 6 and 8. Cardiomyopathy is a condition affecting the cardiac muscle (myocardial). In this case, the muscle walls of the heart chambers are gradually wearing down in terms of structure and function. It is connected with an increase in prefractal dimension [18] and causes difficulty in blood pumping by the heart, resulting in extended intervals between beats (heart failure). It is also important to note that a full understanding of the concept of prefractal dimension and its determination may be useful for distinguishing hypertrophic cardiomyopathy from an athlete's heart, as echocardiography and cardiac magnetic resonance fail to discriminate between the two in some circumstances [19].

Emphysema is characterized by a reduction in prefractal dimension [20]. Figs. 7 and 9 show that when the prefractal dimension decreases, the resistance to fluid flow increases. In other words, under the same pressure, the airflow is reduced, resulting in shortness of breath and fatigue. Low peribronchial emphysema with a prefractal dimension of about 2.7 is associated with increased mortality risk [20], which corresponds to an increase in flow resistance of more than 10% (Fig. 7).

4. Conclusions

Length scale-invariance property characterize many natural and manufactured flow systems. The evaluation of their size and flow resistance is significant and of importance in multi-disciplinary fields. The prefractal theory is appropriated to obtain important insights into the design of these systems. Here, we consider flows of power-law fluids

(Ostwald-de Waele fluid) through porous tubes, and two different flow systems characterized by length scale invariance properties are investigated. First, the highest porosity limit of the walls of porous tubes that can be regarded as having an insignificant impact on the optimal ratio between the sizes of daughter and parent tubes is investigated. Then, a system consisting of Y-shaped tubes – a dendritic flow network - is analyzed. This flow system is characterized by a scaling law between the diameters of the parent tube and the daughter tubes, and the magnification factor of this law is related to the prefractal dimension. Taking as a goal the maximum fluid transport (i.e., minimum flow resistance), and assuming the space occupied by the network is a constant, the value of the prefractal dimension is determined. Expressions for the total size of a network composed of several levels of bifurcating tubes and for its flow resistance can be obtained.

In addition, a system composed of a bundle of tubes is studied. Tubes with tortuous lengths are assumed to exhibit self-similar properties that are scale-independent and statistically consistent at all levels. Thus, power laws are used to characterize the distribution of diameters and lengths. Expressions for the total size and flow resistance are derived in terms of prefractal dimensions.

In summary, these models, which account for the fluid properties and structural characteristics observed in these self-similarity systems, may shed light on an understanding of a variety of flow systems, including hydrology, microfluidic media, and biological systems. The variation in the prefractal dimension that systems can exhibit with the use and with certain illnesses is especially intriguing. A few cases of biological systems are briefly examined.

Acknowledgment

This work was partially supported by funding awarded by FCT - Foundation for Science and Technology, I.P., Projects UIDB/04683/2020 and UIDP/04683/2020.

References

- [1] Harush U, Barzel B. Dynamic patterns of information flow in complex networks, Nature Communications 2017; 8: 2181. https://doi.org/10.1038/s41467-017-01916-3
- [2] Chen S, Miguel AF, Aydin M. Constructal design in the cooling and hydraulic performance of tube heat sinks. International Communications in Heat and Mass Transfer 2021; 129: 105668. https://doi.org/10.1016/j.icheatmasstransfer.2021.105668
- [3] Miguel AF, Rocha LAO. Tree-shaped flow networks fundamentals, in: Tree Shaped Fluid Flow and Heat Transfer, Springer, New York, 2018; 9-34. https://doi.org/10.1007/978-3-319-73260-2 2
- [4] Mandelbrot BB. The Fractal Geometry of Nature, W. H. Freeman and co, San Francisco, 1982.
- [5] Falconer K. Fractal Geometry: Mathematical Foundations and Applications, John Wiley & Sons, Hoboken, 2004. https://doi.org/10.1002/0470013850
- [6] Miguel AF. Low dissipative configuration in flow networks subject to constraints, Physica D 2024; 467: 134269. https://doi.org/10.1016/j.physd.2024.134269
- [7] Miguel AF. A constructal view of prefractal dendritic flow networks using an exergy analysis, International Journal of Exergy 2021; 36: 56 75. https://doi.org/10.1504/IJEX.2021.10040964
- [8] Mourzenko VV, Thovert JF, Adler PM. Macroscopic permeability of three-dimensional fracture networks with power-laws size distribution, Physical Review E 2004; 69: 066307. https://doi.org/10.1103/PhysRevE.69.066307

- [9] Balankin AS. The topological Hausdorff dimension and transport properties of Sierpinski carpets, Physics Letters A 2017; 381: 2801-2808. https://doi.org/10.1016/j.physleta.2017.06.049
- [10] Sahu AK, Roy A. Clustering, connectivity and flow responses of deterministic fractal-fracture networks, Advances in Geosciences 2020; 54: 149-156. https://doi.org/10.5194/adgeo-54-149-2020
- [11] Babadagli T. Unravelling transport in complex natural fractures with fractal geometry: a comprehensive review and new insights, Journal of Hydrology 2020; 587: 124937. https://doi.org/10.1016/j.jhydrol.2020.124937
- [12] Miguel AF, Rosa R, Silva AM. Fractal geometry description of the permeability of a natural fissured rock. Proceedings of 9th International Congress on Deterioration and Conservation of Stone, Elsevier Science BV, 2000; 1: 595-560. https://doi.org/10.1016/B978-044450517-0/50145-8
- [13] Miguel AF. Permeability of fractal porous materials composed of different combinations of capillary tubes, International Journal of Hydromechatronics 2020; 3: 199-212. https://doi.org/10.1504/IJHM.2020.107783
- [14] Miguel AF. Fluid flow in a porous tree-shaped network: optimal design and extension of Hess-Murray's law, Physica A 2015; 423: 61-71. https://doi.org/10.1016/j.physa.2014.12.025
- [15] Middleman S. An Introduction to Fluid Dynamics: Principles of Analysis and Design, Wiley, New York, 1997
- [16] Vassilieff CS. An elliptic filtration variation on Poiseuille-type laminar solutions of Navier-Stokes equations, Journal of Membrane Science 1994; 91: 153-161. https://doi.org/10.1016/0376-7388(94)00030-1
- [17] Harrar K, Hamami L. The fractal dimension correlated to the bone mineral density, Transactions on Signal Processing 2008; 4: 110-126
- [18] Captur G, Karperien AL, Hughes AD, Francis DP, Moon JC. The fractal heart embracing mathematics in the cardiology clinic, Nature Reviews Cardiology 2017; 14: 56-64. https://doi.org/10.1038/nrcardio.2016.161
- [19] Vilades D, Garcia-Moll X, Gomez-Llorente M, Pujadas S, Ferrero-Gregori A, Doñate T, Mirabet S, Leta R, Pons-Lladó G, Carreras F, Cinca J. Differentiation of athlete's heart and hypertrophic cardiomyopathy by the fractal dimension of left ventricular trabeculae, International Journal of Cardiology 2021; 330: 232-237. https://doi.org/10.1016/j.ijcard.2021.02.042
- [20] Bodduluri S, Puliyakote ASK, Gerard SE, Reinhardt JM, Hoffman EA, Newell Jr. JD, Nath HP, Han MK, Washko GR, Estépar RSJ, Dransfield MT, Bhatt SP. Airway fractal dimension predicts respiratory morbidity and mortality in COPD, Journal of Clinical Investigation 2018; 128: 5374-5382. https://doi.org/10.1172/JCI120693